Quarterly Journal of the Royal Meteorological Society Q. J. R. Meteorol. Soc. 141: 285–298, January 2015 A DOI:10.1002/qj.2358

RMetS
Royal Meteorological Society

Effect of small-scale surface heterogeneities and buildings on radiation fog: Large-eddy simulation study at Paris–Charles de Gaulle airport

Thierry Bergot,[a]* Juan Escobar[b] and Valery Masson[a]
[a]*Groupe d'étude de l'Atmosphère Météorologique, Centre National de Recherches Météorologiques, Toulouse, France*
[b]*Laboratoire d'Aérologie, Toulouse, France*

*Correspondence to: T. Bergot, Météo-France, GAME–CNRM, 42 avenue G. Coriolis, F-31057 Toulouse Cedex, France.
E-mail: Thierry.Bergot@meteo.fr

Large-eddy simulations (LES) of radiation fog were performed over an airport area to study the effect of urban canopy on fog. These LES were performed with the Meso-NH research model at very high resolution: 1.5 m in the horizontal and 1 m in the vertical and over a domain 4.5 km × 1.5 km.

The blocking effect of the airport buildings led to strong wind shear and consequently to the production of turbulent kinetic energy (TKE). The airport buildings also had a strong effect on vertical velocity, with a subsidence region behind the buildings. The increase of both turbulence and vertical velocity strongly modified the fog formation. The fog layer took more time to form in the airport area, but the increase in turbulence facilitated the vertical development of the fog layer.

The fog took 1.5 h to form over the whole simulated airport area. The fog height was heterogeneous during the formation phase, with the formation of very low clouds locally. The effect of airport buildings on vertical velocity could explain these heterogeneities of the fog height. During the mature phase of the fog, the buildings had little impact on the fog layer characteristics. The fog dynamics were mainly controlled by processes at its top.

These results suggest that the inclusion of high levels of detail in the building representation remains important for the local forecasting of fog formation. Particularly, small-scale heterogeneities can explain the spatial variability of fog formation. It seems necessary to take small-scale variability of the urban canopy into account for local and accurate forecasts of fog formation over airport areas.

Key Words: radiation fog; large eddy simulation; heterogeneous terrain; buildings

Received 18 November 2013; Revised 24 February 2014; Accepted 24 February 2014; Published online in Wiley Online Library 15 April 2014

1. Introduction

Fog has a strong impact on personal safety and on the economy, especially in the field of transportation. Adverse ceiling and visibility conditions contribute to 35% of the weather-related accidents in the civil aviation sector and cause 168 fatal casualties per year on average (Herzegh *et al.*, 2004). Adverse visibility conditions strongly reduce an airport area's traffic flow. At Paris–Charles de Gaulle (CdG) international airport, adverse visibility conditions lead to the application of Low Visibility Procedures (LVP: horizontal visibility under 600 m or ceiling below 60 m). This halves the efficiency of the airport, causing numerous flight delays. At Paris–CdG, an average of 30 LVP cases occur during a winter season. However, the number of LVP cases strongly depends on the year studied, with a maximum of about 60 LVP cases (Roquelaure *et al.*, 2009).

Unfortunately, numerical weather prediction (NWP) models are usually unable to forecast the exact location and life cycle of a fog layer. Despite all the improvements in horizontal and vertical resolution of 3D mesoscale models, the simulation of fog remains a challenge. The lack of accurate visibility forecasts results from a variety of factors (see e.g. Bergot *et al.*, 2005), including small-scale processes like turbulence and surface heterogeneities. The mechanisms of fog formation, development and dissipation are very complex, including numerous interactions between physical processes involving the land surface, turbulence and cloud microphysics. Efforts have been made to improve our knowledge of these processes, but many of these studies focus on homogeneous surface conditions (Musson-Genon, 1987; Bott *et al.*, 1990; Duynkerke, 1991; Bergot *et al.*, 2005; Clark, 2006). An intercomparison experiment carried out by Bergot *et al.* (2007) and Terradellas and Bergot (2007) revealed significant sensitivity

to turbulence and land–atmosphere interactions. The majority of studies of surface heterogeneity effects have used numerical mesoscale simulations to look at surface heterogeneities at a scale of 10 km (Cuxart and Jimenez, 2012). However, even in homogeneous conditions, fog layers are heterogeneous in nature at a small scale of the order of several hundred metres (Bergot, 2013). Understanding of the local processes involved in a fog layer is currently a challenge toward improving fog forecasts. This goal, however, cannot be reached using current mesoscale models. Progress in this area requires the use of model simulations at metric-scale resolution. It is very important to understand better the temporal and spatial heterogeneities of fog at a very fine scale. This seems essential if the mechanisms of fog formation, development and dissipation are to be dissected.

The properties of the atmosphere near the surface are influenced by the underlying land surface and the prediction of fog is very sensitive to the turbulent fluxes of heat and momentum between the land surface and the atmospheric boundary layer (Bergot and Guedalia, 1994; Clark and Hopwood, 2001). Therefore, the prediction of the spatial distribution of fog layers over heterogeneous land surfaces depends strongly on the prediction of the feedback between the land surface and the atmospheric boundary layer. This is especially true under stable atmospheric conditions (Holtslag *et al.*, 2013), hence further research should focus on heterogeneous surface conditions. The atmospheric boundary layer is characterized by a wide range of length- and time-scales, which are highly dependent on the spatial distribution of the surface properties. Heterogeneous surface conditions can occur at many scales, both naturally and through human modifications. For example, the surface of airports is made up of a patchwork of different complex surfaces, such as grass, runway and buildings of various heights. Such fragmentation induces a 3D variability in micrometeorological fields that may lead to the formation of local meteorological conditions. The complex effect of urbanization in the airport area can have complicated and marked influence on fog. This wide range of complex surfaces disturbs the turbulent flow over the surface and influences the processes that govern the exchange of momentum and heat between the ground and the surface boundary layer. Therefore, these surface heterogeneities over the airport can introduce significant variability in the distribution of a fog layer and have a substantial impact on the ability to forecast fog accurately.

Improving fog prediction for airports requires detailed spatial information about turbulent fluxes. Obtaining this kind of information through measurements is difficult and requires several flux tower measurements or a tethered balloon, both of which are impossible to implement over an airport. Fog research through observational analysis alone is thus insufficient and numerical simulation is a very useful tool, not only for forecasting but also for carrying out research on key physical processes influencing fog life cycles. Moreover, 3D simulations have the advantage of complete spatial and temporal coverage. The large-eddy simulation (LES) has emerged as a very useful tool for exploring the physical mechanisms involved in the boundary layer. LES is a numerical modelling approach that explicitly resolves energy-containing turbulent motions, which are responsible for most turbulent exchanges. A few researchers have used this approach to improve the understanding of fog over homogeneous conditions (Nakanishi, 2000; Porson *et al.*, 2011; Bergot, 2013). In this study, LES modelling at very high resolution is used to capture the main characteristics of the influence of small-scale surface heterogeneities on fog.

This study focuses on radiation fog over an airport area. The impact of terrain heterogeneity on the local life cycle of a radiation fog layer is investigated using a LES model coupled to a land surface model.

The quality of this kind of simulation depends on the horizontal and vertical resolution, as discussed in Beare and MacVean (2004). Here, LES at 1 m vertical resolution and 1.5 m horizontal resolution are used to capture the main characteristics of the development of a fog layer. Sufficient resolution and size are necessary to represent the surface heterogeneities of the airport. For this study, a grid of 3072 × 1024 points is used. To the best of our knowledge, this is the first study of LES fog simulation at this scale taking the representation of buildings into account.

The life cycle of radiation fog can be decomposed into three stages according to the behaviour of the turbulent kinetic energy (TKE): the onset phase, the development phase and the dissipation phase (Nakanishi, 2000). The onset stage is characterized by low intensity of turbulence and a strong inversion near the ground. The development phase is characterized by a strong increase of the TKE and the appearance of a mixed fog layer. Finally, the dissipation stage is characterized by an increase in the unstable stratification of the fog layer, due to surface heating by solar radiation, which leads to the evolution of the fog into stratocumulus. This study focuses on the first two stages of the fog life cycle: the formation and the mature phases. The dissipation phase will be studied in a future article.

In section 2, the model used and the simulations are presented. Section 3 shows the results of simulations for homogeneous surface conditions. Sections 4 and 5 focus on the impact of the airport heterogeneities on the fog layer. The small-scale structures of the fog layer at Paris–CdG airport are presented in section 6. Finally, some conclusions are drawn and perspectives evoked in section 7.

2. Model description and experimental design

2.1. Model description

The large-eddy model used here is the non-hydrostatic anelastic research model Meso-NH.* The configuration chosen for this study was similar to the one used in Bergot (2013). As a subgrid-scale model, a 3D turbulent scheme with a prognostic TKE (Cuxart *et al.*, 2000) and a Deardorff mixing length (Deardorff, 1980) is used. The radiative transfer is computed by solving long-wave and short-wave radiative transfers separately using the European Centre for Medium-Range Weather Forecasts (ECMWF) operational radiation code (Morcrette, 1991).

For the microphysics, the model includes a one-moment bulk microphysical scheme. The liquid cloud water is calculated prognostically but condensation and evaporation are assumed to be instantaneous. No ice was considered, given the temperature of the fog layer. The droplet sedimentation is computed by considering Stokes law for the cloud droplet sedimentation velocity and assuming that the cloud droplet size distribution follows a generalized gamma function:

$$n_c(D) = N\frac{\alpha}{\Gamma(\nu)}\lambda^{\alpha\nu}D^{\alpha\nu-1}\exp[-(\lambda D)^{\alpha}], \tag{1}$$

where

$$\lambda = \left(\frac{\pi}{6}\rho_w\frac{\Gamma(\nu+3/\alpha)}{\Gamma(\nu)}\frac{N}{\rho_a r_c}\right)^{1/3}. \tag{2}$$

Here, Γ is the gamma function, D the cloud droplet diameter, N the number of cloud droplets, r_c the cloud liquid water content and ρ_w and ρ_a the density of liquid and atmosphere, respectively. α and ν are parameters allowing distribution fitting. These parameters were adjusted using typical fog droplet spectra (Pawlowska and Brenguier, 2000; Remy, 2006; Rangognio, 2009): $\alpha = 3$, $\nu = 1$ and $N = 300\,\mathrm{cm}^{-3}$.

The atmospheric part of the model is coupled with the Surface Externalisée (SURFEX) interactive land-surface scheme†

*http://mesonh.aero.obs-mip.fr
†http://www.cnrm.meteo.fr/surfex/

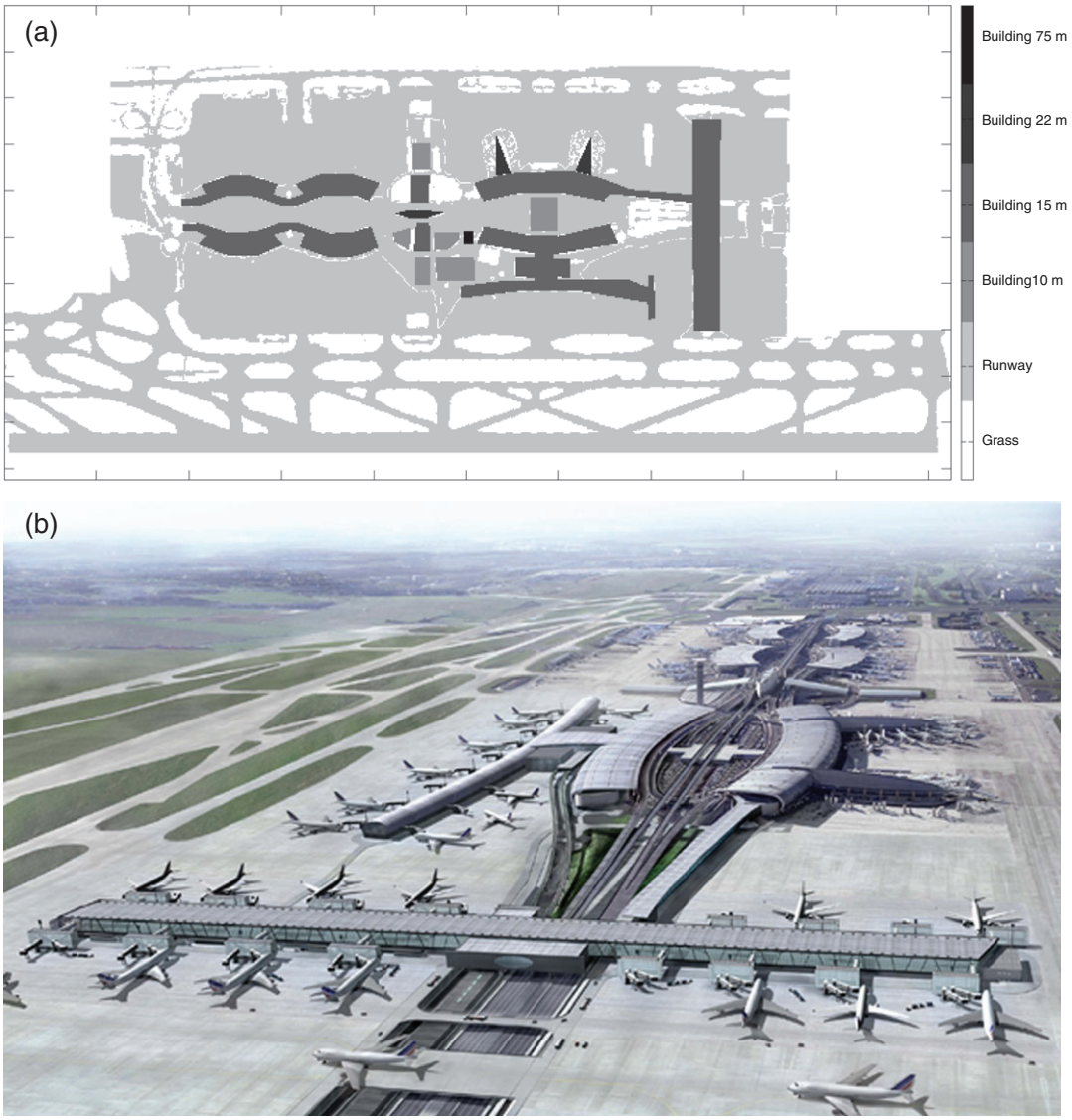

Figure 1. (a) The airport representation used for the simulations and (b) an artist's impression of the airport.

Table 1. Urban parameters used for the BLD and DRAG simulations.

	Building	Building	Building	Building	Road
Height (m)	10	15	22	75	0.1
Roughness length (m)	1	1.5	2.2	7.5	0.01
Albedo roof	0.15	0.15	0.15	0.12	
Albedo wall	0.25	0.25	0.25	0.25	
Albedo road					0.08
Emissivity roof	0.90	0.90	0.90	0.90	
Emissivity wall	0.85	0.85	0.85	0.85	
Emissivity road					0.94
Surface temperature (K)	281	281	281	281	281
Inside temperature (K)	295	295	295	295	285

(Masson *et al.*, 2013). SURFEX includes the Interaction between Soil, Biosphere and Atmosphere (ISBA) model (Noilhan and Planton, 1989) for natural covers and the Town Energy Balance (TEB) urban canopy model (Masson, 2000) for built-up covers. Both surface models compute the exchanges of heat, water and momentum between surfaces and the atmosphere. SURFEX has been validated against numerous field data (see http://www.cnrm.meteo.fr/surfex/ for references). TEB simulates the exchanges of the surface and buildings with the atmosphere above and computes the conduction and convection (heat and water) fluxes and momentum fluxes, together with radiative exchanges. A simplified version of TEB is used for this study, because the street-canyon hypothesis cannot be used to represent urban canopy at a 1 m scale. The temperature evolution of the walls and roof of airport buildings and the roads (here runways) is based on energy budget considerations. This allows us to study the thermal effect of the urban airport canopy on fog. The momentum fluxes in the simplified TEB version are computed following a roughness-length formulation.

In complex terrain, like an airport, the influence of surface elements (e.g. buildings of different heights and shapes) is currently taken into account through surface schemes like SURFEX. In these land-surface schemes, the effects of the buildings on the flow is parametrized using a roughness approach and the influence of buildings is represented through a gridded roughness length. However, it is well known that the roughness

Table 2. Characteristics of the simulations performed.

Name	Natural surface	Urban surface	Horizontal domain	Horizontal resolution (m)	Vertical resolution (m)	Time (s) step
REF	ISBA	None	1024 × 1024	1.5	1 m	0.1
BLD	ISBA	Simplified TEB	2048 × 1024	1.5	1 m	0.1
DRAG	ISBA	Simplified TEB + DRAG	3072 × 1024	1.5	1 m	0.05

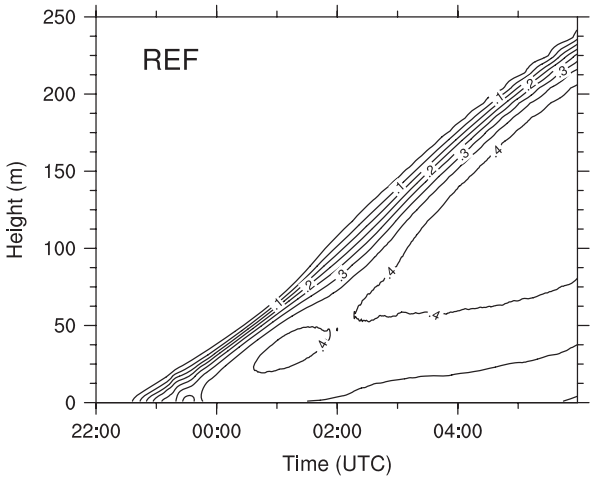

Figure 2. The time–height cross-section of the simulated mean liquid water content ($g\,kg^{-1}$) for the REF simulation.

approach is unsatisfactory if the vertical and horizontal sizes of the first layers are not large enough (Bou-Zeid *et al.*, 2009). For simulations at a resolution of 1 m using a heterogeneous surface, this approach cannot explicitly resolve the buildings in the airport region and thus misses important three-dimensional heterogeneous processes that can have a strong impact on TKE. In this study of a real airport, it is important to represent the complexity of the dynamic variables due to the buildings properly, so the drag approach of Meso-NH is used. It consists of introducing an additional term in the momentum and TKE equations. This term is modelled as a force oriented in the opposite direction to the flow. The drag approach has been tested in stable LES for a vegetation canopy (Aumond *et al.*, 2013), and extended to a building canopy (Hamdi and Masson, 2008) as in Brown (2000) and Carissimo and Macdonald (2001). The additional terms in the momentum equation are as follows:

$$\frac{\partial u}{\partial t}\,|_{\mathrm{DRAG}} = -C_{\mathrm{d}} A u \sqrt{u^2 + v^2}, \tag{3}$$

$$\frac{\partial v}{\partial t}\,|_{\mathrm{DRAG}} = -C_{\mathrm{d}} A v \sqrt{u^2 + v^2}, \tag{4}$$

$$\frac{\partial e}{\partial t}\,|_{\mathrm{DRAG}} = -C_{\mathrm{d}} A e \sqrt{u^2 + v^2}, \tag{5}$$

where u and v are the wind components, e the TKE, C_{d} the drag coefficient and A the reference area of canopy. In this study, we assumed that the product of the drag coefficient and the reference canopy area was vertically constant and equal to 1000 inside the buildings. Unlike trees, buildings are not porous but constitute rigid obstacles to the flow.

2.2. Surface conditions

The construction of the surface conditions is one of the major steps in setting up the calculation of a very fine mesh simulation. In most cases, the exact dimensions, location and details of buildings and runways are not easily available. For this study, the actual structure of the buildings was supplied by Aéroport de Paris; see Figure 1. The real airport surface was idealized into six different classes. No topography was considered. The idealized urban cover (Figure 1) accounted for the runway and buildings of four different heights (10, 15, 22 and 75 m). The majority of buildings are accounted for explicitly here; only a few small buildings were not included. The cover was simplified and runways outside the urban domain were not considered. The urban domain covered an area of 4.5 km × 1.5 km. The cover outside the aiport canopy was assumed to be composed only of grass. Despite these simplifications, the characteristics of the airport area at a small scale are very realistic and are believed appropriate to study the importance of the main urban area of Paris–CdG for fog. This is one of the first times that a realistic surface representation at a few metres of resolution has been used

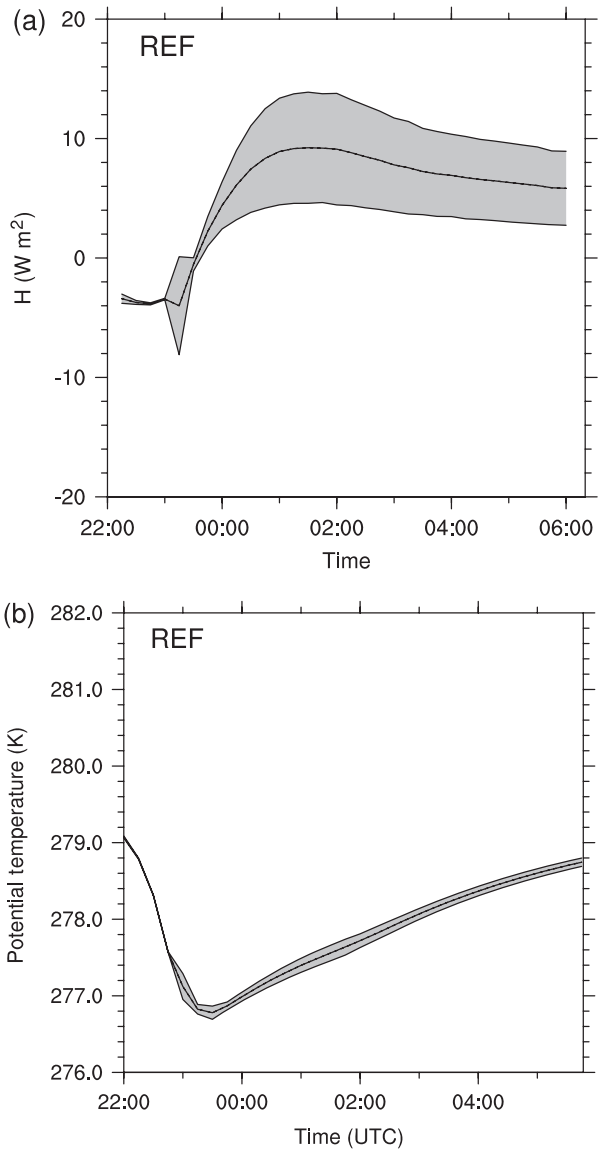

Figure 3. Time series of (a) ground sensible heat flux and (b) temperature at 2 m for the REF simulation. Mean values over the simulation domain are shown with solid lines and the dispersion is indicated by grey areas.

to perform numerical simulation of fog. The parameters that characterize the urban environment are given in Table 1.

2.3. *Description of the case studied*

The atmospheric forcing conditions simulated here are the same as the case studied in Bergot (2013) A detailed description of this case, which occurred during the night of 18–19 February 2007, can be found in Bergot (2013) and only the main properties of this fog event are presented in this article. This event can be classified as a radiative fog event. The visibility fell to less than 1000 m around 2240 UTC. Over the next 30 min, the downwelling long-wave radiative flux increased by 65 W m^{-2} at the surface and the stable surface layer was eroded. The fog height was more than 200 m during the mature phase, but it was very difficult to define the fog top precisely from the available observations. Significant variation was observed in the inversion height, as observed in the temperature profiles during the night. The wind speed at the top of the atmospheric boundary layer was moderate, between 8 and 10 m s^{-1}. However, during the fog event, the wind profile showed strong variation at the top of the fog layer. The fog dissipated at ground level at 0800 UTC, gradually lifting into stratocumulus clouds.

The previous LES study in homogeneous conditions (Bergot, 2013) showed that the model really resolves the large eddies and this feature will not be studied in detail in the present article. Bands in liquid water content (LWC) appeared during the formation phase, leading to a burst in TKE. These structures were induced by Kelvin–Helmholtz (KH) instability due to a large wind shear at the top of the surface inversion. During the mature phase of the fog, waves appeared at the top of the fog layer. This induced substantial variability in the thermodynamic parameters in the upper third of the fog layer, associated with large TKE. The dissipation phase was characterized by an increase in the spatial variability of the fog liquid water. In consequence, the dissipation of the fog layer at ground level was not uniform and took about 2 h.

2.4. *Simulation set-up*

The model was initialized before the fog formation at 2100 UTC and the simulation covers the period until 0600 UTC. Three simulations were performed: in the first, called REF, the ground was specified as homogeneous and only composed of grass; in the second, called BLD, the heat fluxes and friction due to buildings and runway were simulated using the simplified version of the TEB parametrization, as described in section 2.1; finally, in the third, called DRAG, a more realistic effect of the urban canopy on the wind was simulated using the surface parametrization including the additional drag terms related to the presence of buildings, as described in section 2.1. To reduce the computational cost, the horizontal domain was set to 1024 × 1024 grid points for the REF simulation, 2048 × 1024 for the BLD simulation and 3072 × 1024 for the DRAG simulation. The influence of the domain size will be discussed in section 3. The lateral boundary conditions

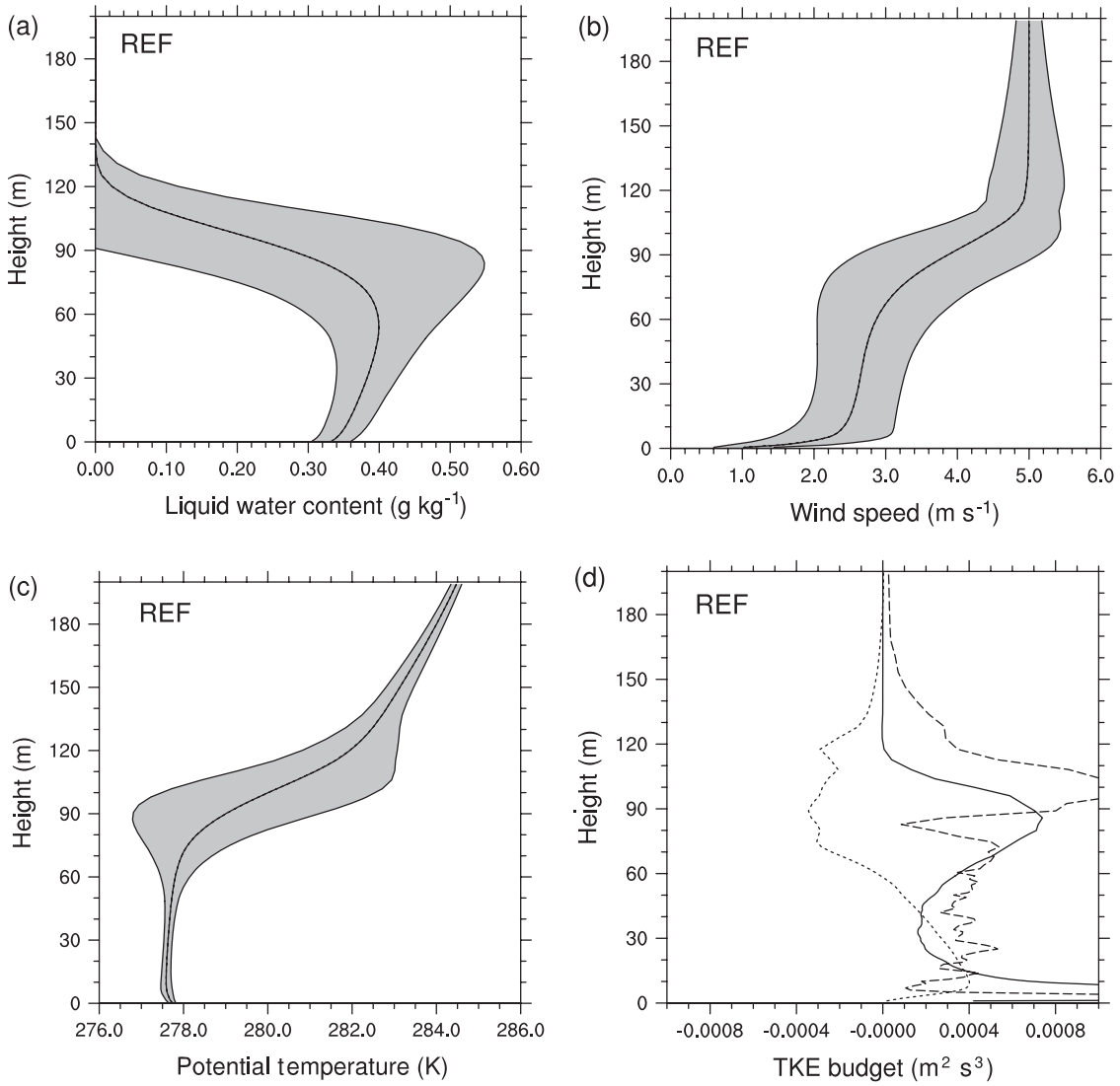

Figure 4. Vertical profiles for the REF simulation at 0215 UTC of (a) liquid water content, (b) wind speed and (c) temperature. Mean values over the simulation domain are shown with solid lines and the dispersion is indicated by grey areas. (d) TKE budget: dynamic production (solid line), transport (dashed line) and buoyancy term (dotted line).

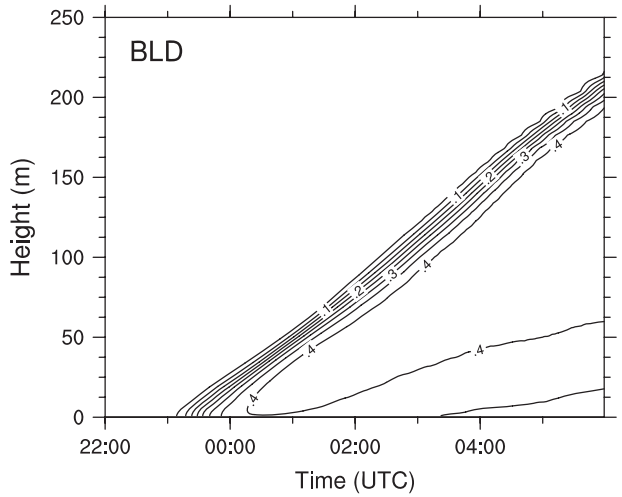

Figure 5. Same as Figure 2, but for the BLD simulation.

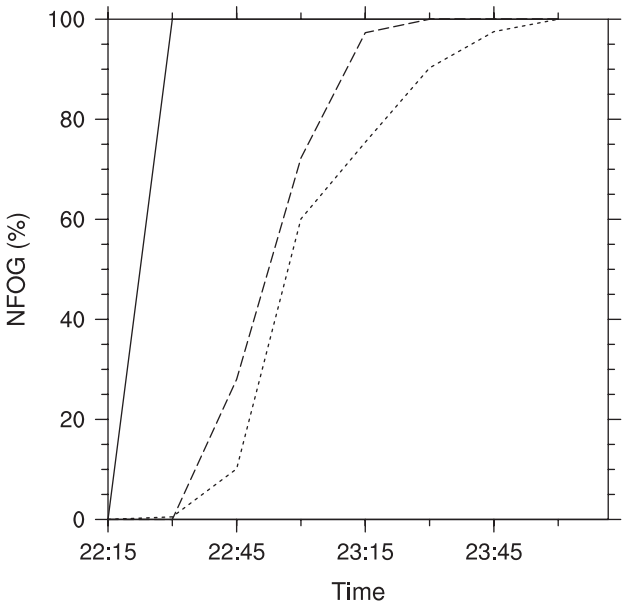

Figure 6. Time evolution of the fraction of fog for the three simulations: REF (solid line), BLD (dashed line) and DRAG (dotted line).

were periodic. The horizontal domain was extended in the wind direction in order to minimize the effect of the lateral conditions for BLD and DRAG simulations. The horizontal resolution was set to 1.5 m and the vertical resolution was 1 m for the first 50 points nearest the ground, increasing slightly up to the top of the model; 135 vertical levels were used. The time step varied from 0.1 s for REF and BLD simulations to 0.05 s for the DRAG simulation. The reduction of the time step is due to stronger wind shear near the buildings in the DRAG simulation. Table 2 summarizes the different model configurations for the three simulations. In order to generate turbulence, white noise of 0.5 K was applied to the first 50 m in the initial conditions.

3. Fog in homogeneous conditions

In this section, the surface conditions are homogeneous and the surface consists only of grass. This simulation is called REF. Figure 2 shows the time–height cross-section of the simulated mean LWC of the fog layer for the REF simulation. The evolution of the fog layer is similar to that simulated by Bergot (2013). The fog began at the ground at about 2230 UTC on average. A burst of TKE appeared near the ground at around 2315 UTC (not shown), due to KH instabilities. These KH billows influenced the dynamical conditions and allowed the fog to develop vertically. After 0100 UTC, the TKE had the largest value at the top of the fog layer. These results show that the decrease in resolution and increase in domain size between Bergot (2013) and this study had little impact on the fog simulation. The energy fluxes at the ground drove the formation phase of the fog. To illustrate this point, the sensible heat fluxes are plotted in Figure 3(a). Until 2300 UTC, the energy balance at the ground is typical of clear-sky conditions, with very slight spatial variability. The appearance of KH billows near the ground at around 2315 UTC perturbed the sensible heat fluxes and induced a sudden dispersion of about 8 W m^{-2}. After this time, the fog layer became optically thick and a rapid change in the surface energy balance appeared. In particular, the sensible heat flux became positive and there was a significant change in the static stability near the ground, from stable to unstable conditions. The sensible heat flux at the ground was maximum near 0200 UTC, with a value of about 10 W m^{-2}. Afterwards, it decreased slowly but the spatial variability remained significant. The evolution of the temperature at 2 m is plotted in Figure 3(b). The temperature dispersion at the ground was small, about 0.1 K, throughout the fog life cycle. The temperature at the ground was minimum at 2330 UTC and increased by about 2.5 K during the night, due to the radiative effect of the fog layer.

Waves in LWC were clearly seen at the top of the fog layer, with a horizontal scale of about 350 m, between three and four

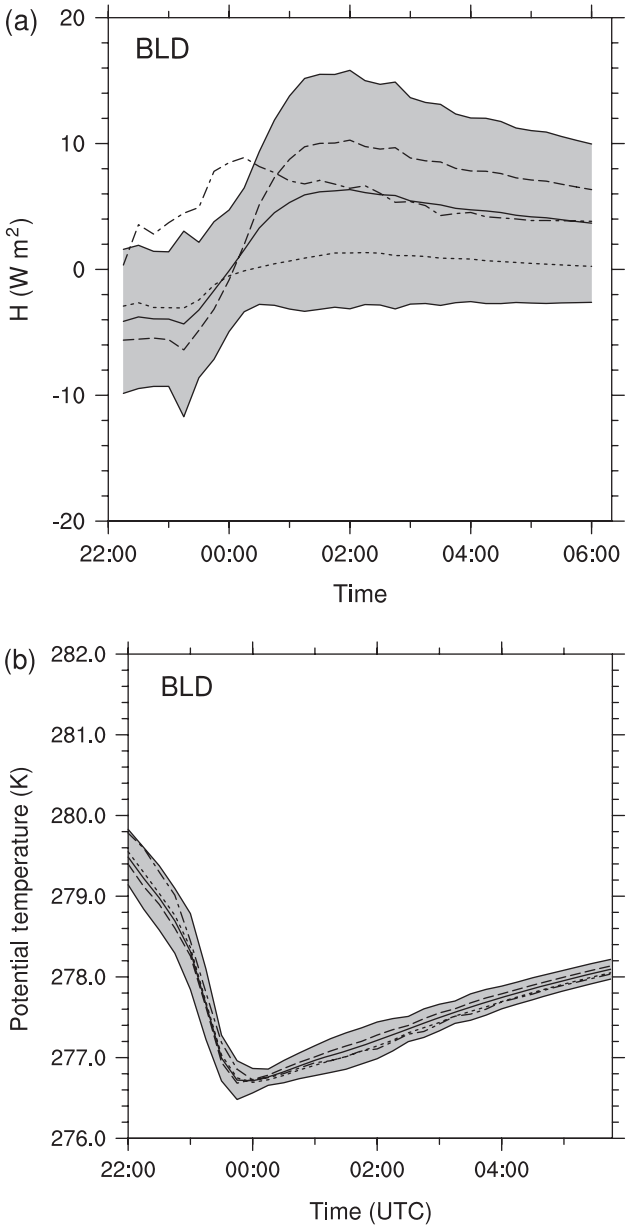

Figure 7. Same as Figure 3, but for the BLD simulation. Means are shown over the simulation domain (solid line), over the grass (dashed line), over the runways (dotted line) and over the buildings (dot–dashed line).

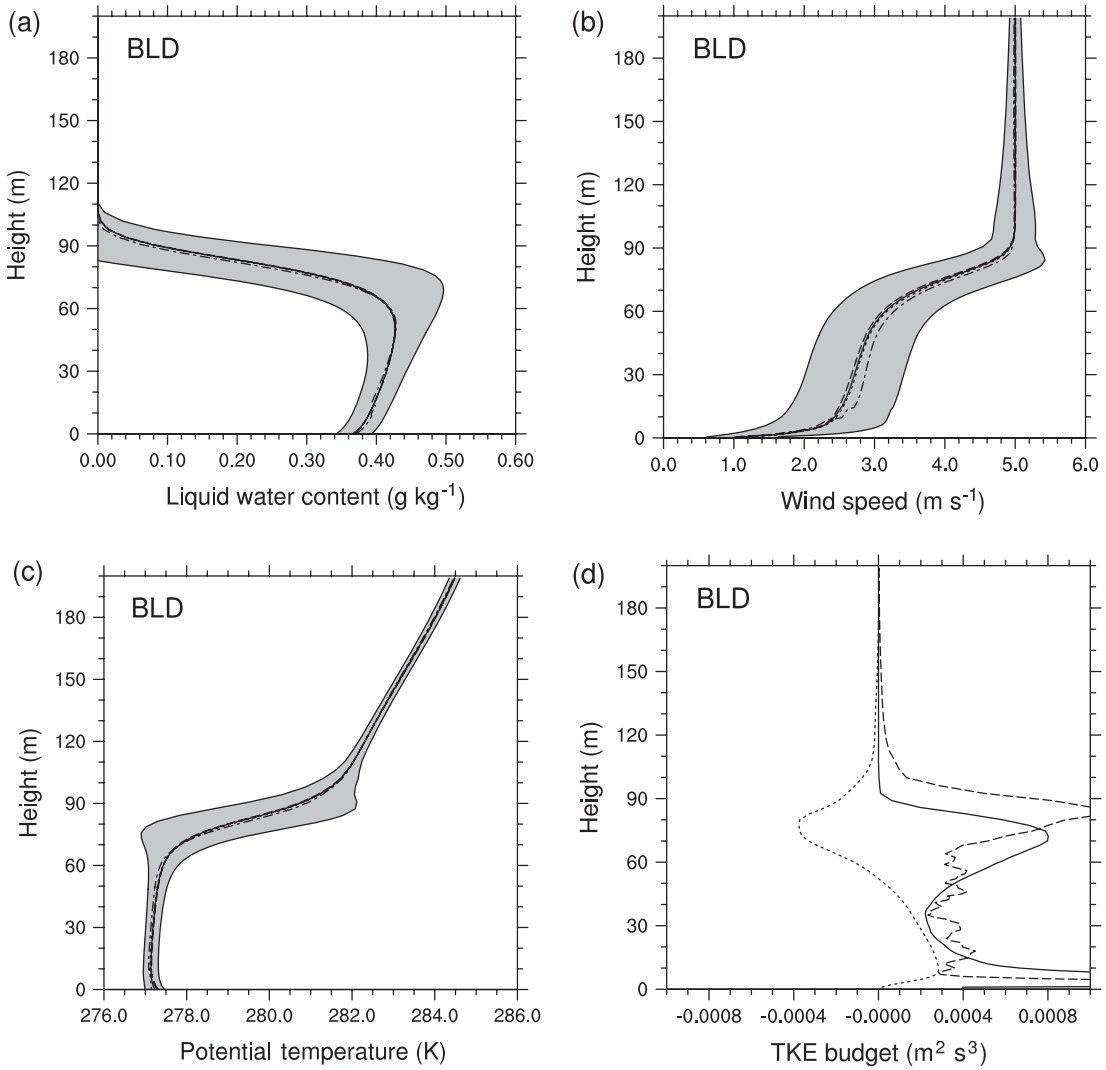

Figure 8. Same as Figure 4, but for the BLD simulation. (a)–(c) Means over the simulation domain (solid line), over the grass (dashed line), over the runways (dotted line) and over the buildings (dot–dashed line). (d) TKE budget over the simulated domain: dynamic production (solid line), transport (dashed line) and buoyancy term (dotted line).

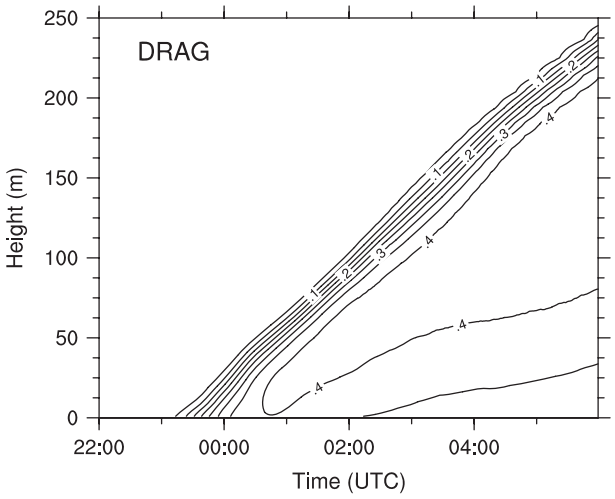

Figure 9. Same as Figure 2, but for the DRAG simulation.

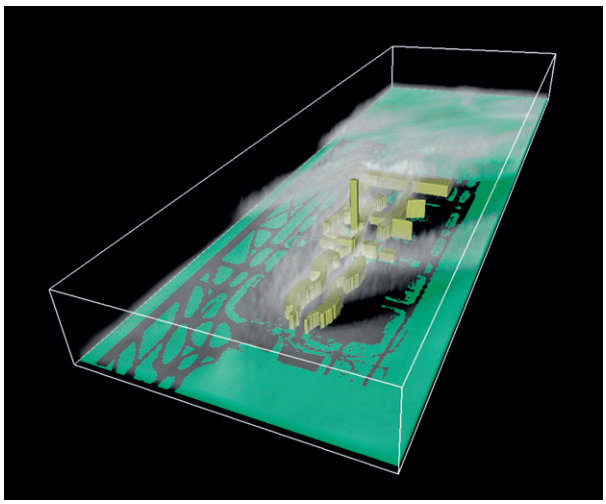

Figure 10. 3D view of the simulated fog layer at 2300 UTC for the DRAG simulation. The buildings are in yellow, the runways are in black and the grass is in green.

times the fog top height (not shown). The fog top height varied substantially between 90 and 140 m, i.e. by about a third of the fog depth. The value of the wavelength was in agreement with the observations by Uematsu *et al.* (2005) and with the previous study by Bergot (2013). As shown in Bergot (2013), the large vertical wind shear at the top of the fog layer (Figure 4(b)) associated with the inversion led to a Richardson number close to the critical value (0.25). This indicates that these structures at the top of the fog layer are induced by KH instabilities. To illustrate the characteristics of the fog layer at 0215 UTC, Figure 4 shows the profiles of mean LWC, wind speed and potential temperature, with the dispersion superimposed. The spatial variability of the LWC is minimum at the ground (around 0.05 g kg^{-1}) and increases in the middle of the fog layer to reach

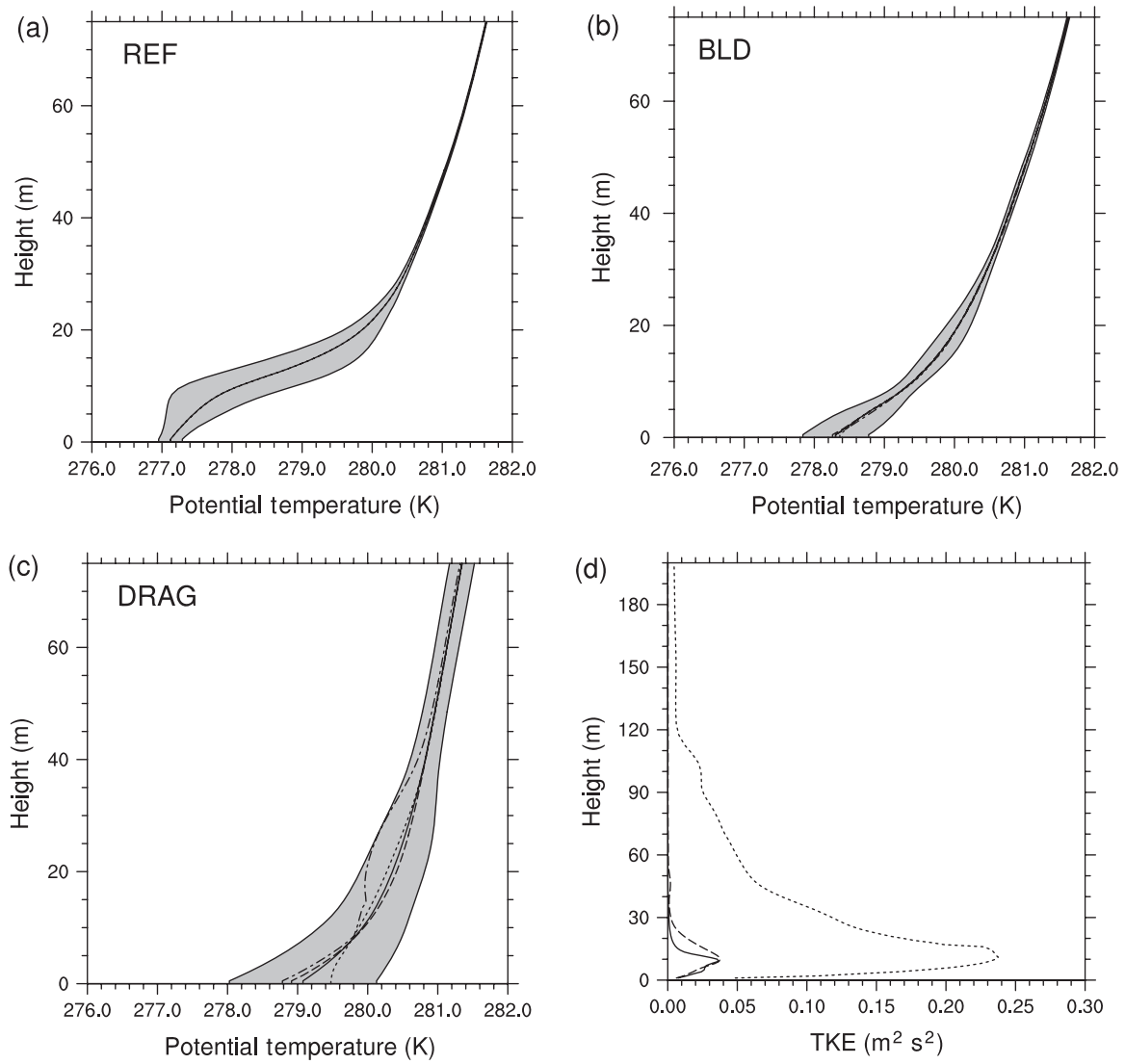

Figure 11. Vertical profiles of temperature at 2315 UTC for (a) REF, (b) BLD and (c) DRAG simulations. Mean values are shown over the simulation domain (solid line), over the grass (dashed line), over the runways (dotted line) and over the buildings (dot–dashed line). (d) Vertical profiles of TKE at 2315 UTC for REF simulation (solid line), BLD simulation (dashed line) and DRAG simulation (dotted line).

about 0.2 g kg^{-1}. In the upper third of the fog layer, the fog is patchy, leading to large spatial variability. The fog layer was practically isothermal, with a very small spread of temperature in the lower half. The spatial variability of temperature increased substantially in the upper third of the fog layer, reaching about 2 K. These fog layer structures were induced by the vertical circulation at the top of the fog layer. To understand better the production of turbulence at the fog top, the TKE budget is shown in Figure 4(d). The TKE budget shows that most of the turbulence at the top of the fog layer is generated by dynamic production due to the wind shear across the fog top and by transport across the inversion. The motions at the top of the fog and the wind shear across the inversion are major processes in the evolution of the fog layer, which is thus controlled by the processes at its top during the mature phase.

4. BLD simulation

In this section, the buildings and runway heat fluxes and friction are simulated in the land surface scheme, as described in section 2.1. Figure 5 illustrates the time–height cross-section of the mean LWC of the fog layer for this BLD simulation. The fog layer appeared at the ground at about 2300 UTC on average, 30 min later than in REF. The vertical growth of the fog layer was smaller and the fog height reached about 215 m at 0600 UTC. The layer was thus 25 m thinner on average than in REF. The billows during the formation time were not conspicuous in the LWC, but could be seen in the TKE (not shown). Classically the LWC was initially maximum near the ground. When the fog became optically thick, the position of the LWC maximum rose, moving close to the fog top. One of the most interesting points concerns the heterogeneity of the fog layer during the formation phase. To illustrate the fog heterogeneity, the fraction of fog at ground level at different times

Table 3. LWP (g m^{-2}) for the three simulations. Values indicated are the mean results, with standard deviation over the simulation domain in the brackets.

Time (UTC)	REF	BLD	DRAG
2300 UTC	1.97 (0.01)	0.10 (0.13)	0.05 (0.09)
0000 UTC	11.3 (0.64)	7.0 (1.30)	6.1 (1.65)
0100 UTC	23.1 (1.78)	19.1 (1.87)	22.0 (2.68)
0200 UTC	34.4 (5.87)	30.6 (2.96)	35.5 (3.46)
0300 UTC	47.8 (4.85)	42.8 (3.18)	48.8 (5.01)
0400 UTC	62.9 (3.62)	55.8 (3.11)	63.2 (4.37)
0500 UTC	75.9 (2.91)	69.1 (2.60)	77.1 (3.89)
0600 UTC	86.4 (3.66)	80.0 (2.41)	88.0 (3.73)

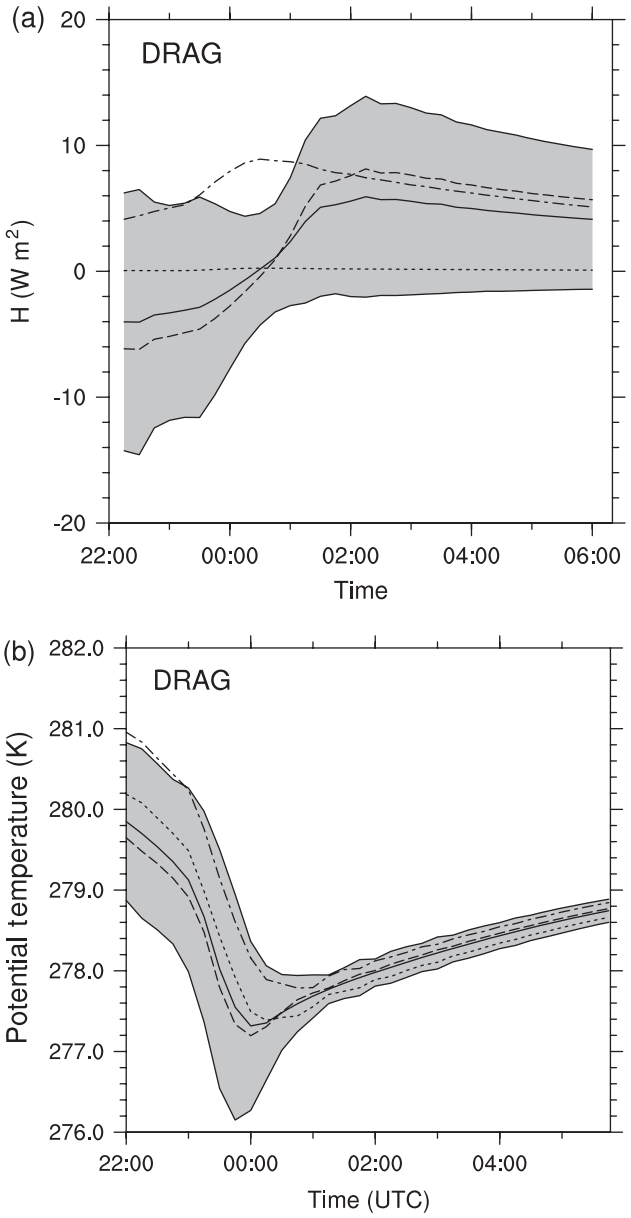

Figure 12. Same as Figure 7, but for the DRAG simulation.

is plotted in Figure 6. While the formation of the fog layer over the entire model domain was quasi-instantaneous for the REF simulation, it took about 1 h for BLD. The fog layer affected all the grid points only at about 2330 UTC. During the formation time, the fog layer was heterogeneous, with grid points free of fog and grid points where the fog layer was more than 10 m high.

The mean sensible heat fluxes over the model domain are plotted in Figure 7(a). The appearance of KH billows near the ground around 2300 UTC can be seen in the sensible heat fluxes, with an increase of dispersion of about 4 W m^{-2}. The major difference with respect to the REF simulation is the spatial variability of the ground sensible heat flux during the formation of the fog layer. The sensible flux is always positive over the buildings, while the difference between grass and runway is about 3 W m^{-2} during the formation phase for a mean value over the model domain of 4 W m^{-2}. As in REF, the sensible heat flux at the ground is maximum near 0200 UTC but the mean value over the model domain is smaller (about 5 W m^{-2}), with stronger dispersion.

The evolution of the temperature at 2 m is plotted in Figure 7(b). A dispersion of 0.7 K can be observed during the formation, with warmer temperatures above the buildings. This has a strong impact on fog formation and could explain the heterogeneity of the fog layer. The spatial variability in the temperature remains higher for the BLD simulation than for the REF one during the fog life cycle. It also has an impact on the mean temperature; BLD is cooler than REF, the difference being about 0.75 K at the end of the night. This difference can be explained by the difference in the optical depth of the fog between the two simulations.

Waves are present at the top of the fog layer with a horizontal scale of about 350 m, as in the REF simulation (not shown). The variability of the fog top height was smaller, between 85 and 110 m, about half that found in REF. The differences are mainly a consequence of the release of heat by the buildings, which slows down the formation of the fog layer. Figure 8 shows the profiles of mean LWC, wind speed and potential temperature, with the dispersion at 0215 UTC superimposed. The LWC and wind speed near the surface are very similar to those in REF. The major difference at ground level is an increase in the spatial variability of the temperature. Associated with the decrease in variability of the fog top, a decrease can be observed in the variability of the temperature, LWC and wind speed at the top of the fog layer. The TKE budget is similar to that in REF, except for stronger thermal damping of TKE at the fog top. The turbulence was mainly dominated by the production at the top generated by wind shear and by transport across the cloud top. It was mainly decoupled from the ground.

5. Impact of 3D obstacles

In this section, the buildings were simulated using the DRAG parametrization (see section 2.1) and the simulation is thus called DRAG. The time–height cross-section of the mean LWC of the fog layer is plotted in Figure 9. The fog appears at ground level around 2300 UTC on average, at the same time as the BLD simulation. However, the vertical development of the fog layer is more rapid and the fog top reaches about 250 m at 0600 UTC, 35 m higher than in BLD but similar to REF. The mean values of LWC over the domain are similar in the three simulations. The major difference concerns the heterogeneity of the fog layer during the formation phase (Figure 10). The appearance of the fog in the whole airport area is very heterogeneous and it takes about 1 h 30 min to cover the entire domain at ground level, 30 min more than for the BLD simulation (Figure 6).

The profiles of temperature during the formation phase are plotted in Figure 11 for the three simulations. The ground temperature is strongly modified (about 2 K) by the presence of the airport, not only by anthropogenic sources (difference between REF and BLD) but also by the change in atmospheric turbulence. The increased turbulence (Figure 11(d)) in the DRAG simulation leads to a reduction of the inversion strength. The maximum of TKE near the ground, due to shear, is about four times larger for the DRAG simulation. Strong shear in the airport area increases the production of TKE. Both the mean flow and the turbulence are distorted by the interactions with the airport buildings. The variance of the temperature profile increases clearly for the DRAG simulation, with an effect not only at ground level but also at the inversion level. KH instabilities are no longer clearly visible during the formation phase for DRAG, in contrast to REF.

To illustrate the evolution of the fog, the liquid water path (LWP) is calculated in Table 3 for the three simulations. It can be seen that the LWP is smaller for the DRAG simulation during the formation phase. However, the LWP increases more rapidly during the mature phase for DRAG and becomes larger than for REF and BLD. This demonstrates that the fog layer takes more time to form in the airport area; however, afterwards the increase in turbulence (see the dispersion of LWP, for example) facilitates the development of the fog layer.

The sensible heat fluxes H are plotted in Figure 12(a). The spatial variability increases strongly before the fog formation, due to an increase in the turbulence. It is also noteworthy that H takes more time to increase during the formation phase. This also reveals that the formation phase is longer. The evolution

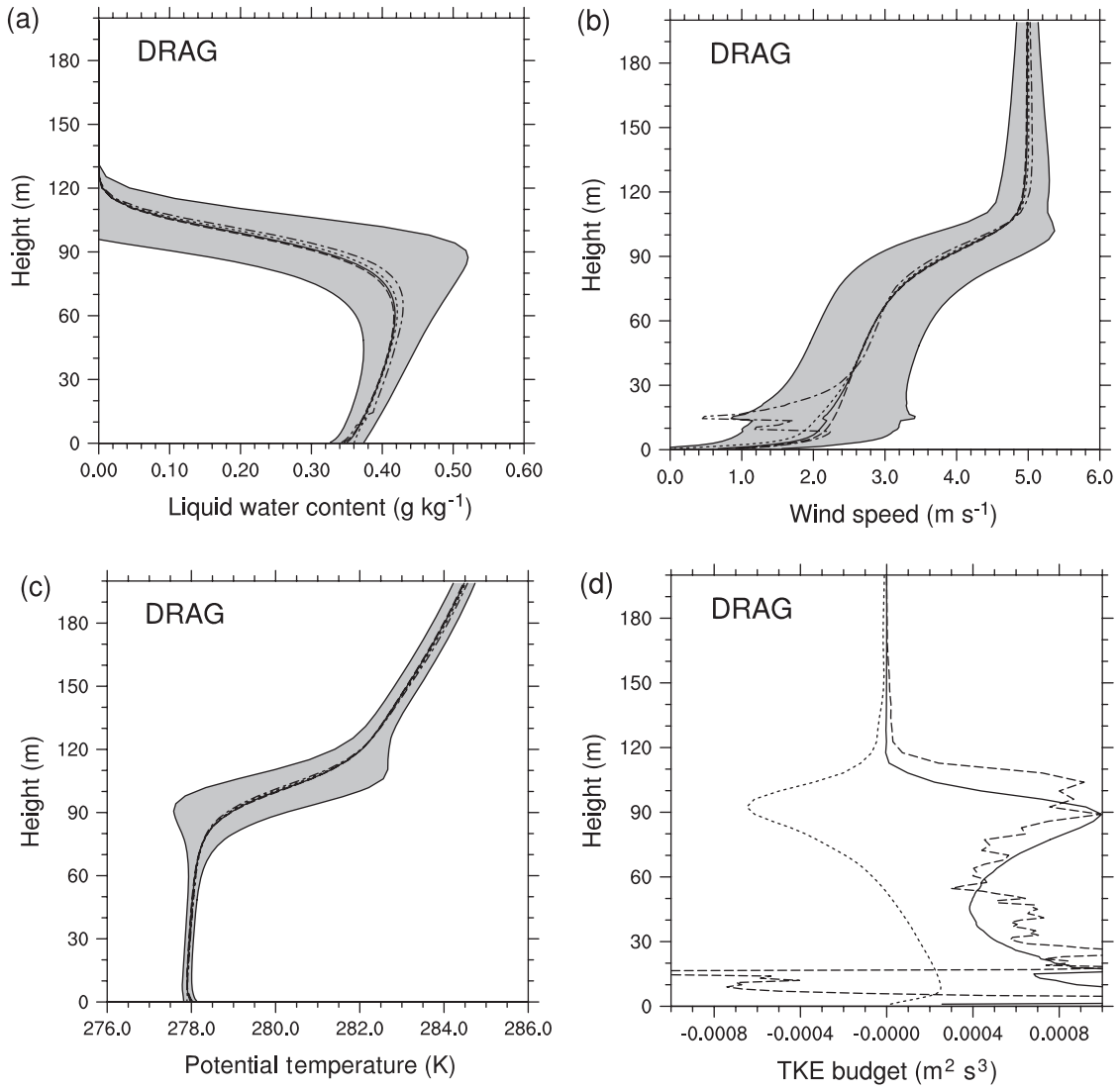

Figure 13. Same as Figure 8, but for the DRAG simulation.

of the temperature at 2 m is plotted in Figure 12(b). As before, the spatial variability is strongly increased during the formation phase with respect to the previous experience. However, once the fog layer is formed, the spatial variability in ground temperature decreases markedly and becomes identical to values obtained in the BLD simulation.

To illustrate the structure of the fog layer during the mature phase, the vertical profiles of LWC, wind and potential temperature at 0215 UTC are plotted in Figure 13. Except for an increase of the dispersion at the fog top with respect to the BLD simulation, the mean and variance of the LWC and temperature are similar. The KH instabilities at the top of the fog layer are less clear than for the REF simulation, showing that these instabilities are very sensitive to wind shear. The major difference between DRAG and BLD concerns the wind profile. The wind velocity is reduced inside the fog layer, showing the blocking effect of the airport buildings. The TKE budget is plotted in Figure 13(d). The production term related to wind shear is slightly increased with respect to BLD, while the damping due to buoyancy is slightly smaller. The dynamic production of TKE increases significantly near the ground, due to the effect of buildings. However, during the mature phase of the fog, its dynamics are mostly dominated by the processes at the top of the fog layer, as for the REF and BLD simulations.

6. Fine-scale structure of fog at airport

The goal of this section is to illustrate the small-scale structure of the fog layer within the airport area. The simulation used is DRAG, which takes both the thermal and dynamic effects of the airport structures into account. The parameters (wind, LWC, vertical velocity, etc.) are averaged over fluid grid cells of 128 points (192 m). Note that points inside the buildings are not considered in this average. The mean over 192 m considered here corresponds to the mean scale of the maximum of energy production (Bergot, 2013).

The mean LWC at 2315 UTC, during the formation phase of the fog, is plotted in Figure 14. Flow patterns in the airport area are strongly modified by the presence of buildings: due to their blocking effect, the atmospheric flow is diverted eastwards and over the airport area. A positive vertical velocity appears upstream and subsidence is found behind the buildings. This induces a vertical oscillation of the wind around the inversion level at a length-scale of about 500 m. The streamwise velocity is significantly reduced over the airport buildings. The transport of LWC has a clear impact on the formation of the fog layer. The fog layer is transported eastward and upward with respect to the airport buildings and can lead to the formation of very low clouds in the inversion level. The effect of the terminal can be clearly seen, with no fog downstream of the buildings. The fog top is generally higher upstream of the buildings. Small-scale variabilities of the fog top also appear on the eastern side of the domain, crosswise to the wind just beyond the main terminal.

The mean vertical velocity is plotted in Figure 15. Upstream of the buildings, the flow is diverted upwards, producing a positive vertical velocity of about $0.1\,\mathrm{cm\,s^{-1}}$. A subsidence region of about $-0.1\,\mathrm{cm\,s^{-1}}$ clearly appears behind the buildings where the flow near the surface accelerates, drawing air from above.

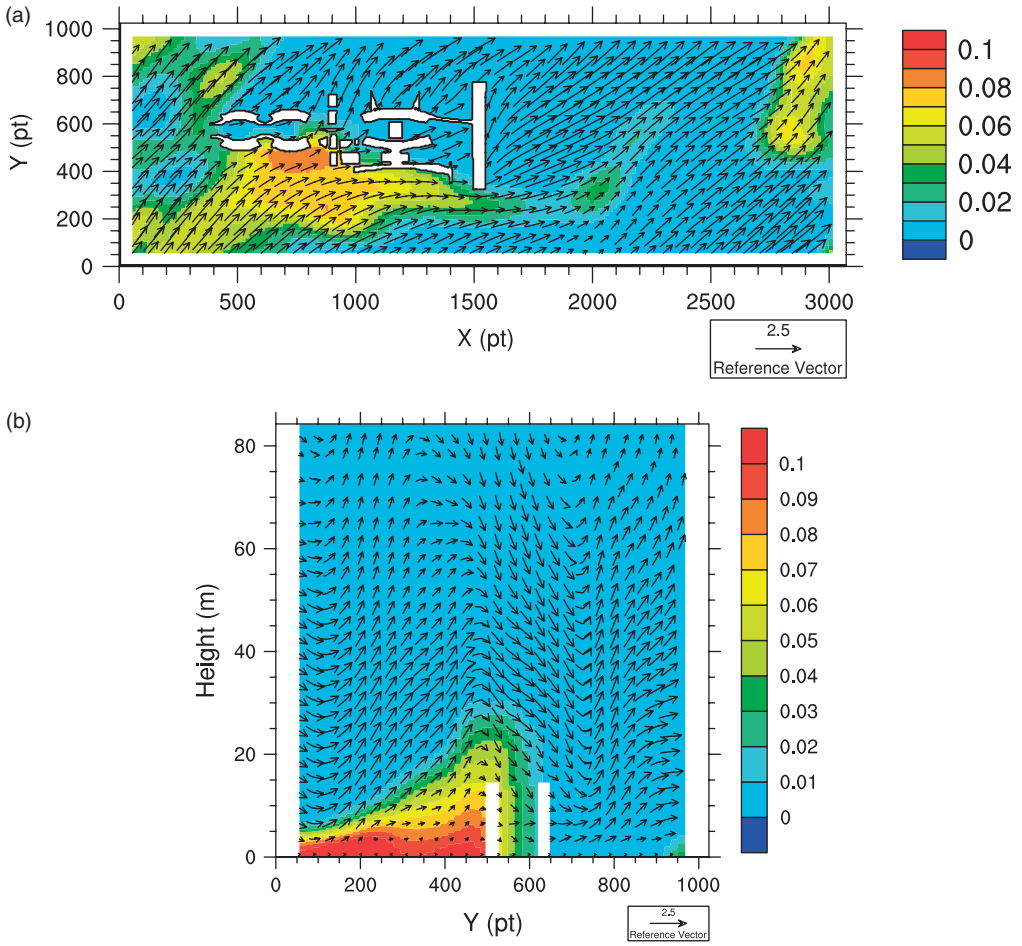

Figure 14. (a) Horizontal cross-section of liquid water content superimposed with the wind at 2315 UTC at 10 m height. (b) Vertical cross-section of liquid water content along the *y*-axis.

This effect of airport buildings on vertical velocity can explain the heterogeneities in the fog height. The strong shear of wind close to the airport buildings leads to the production of TKE. An area of high TKE (about 1 $m^2 s^{-2}$) can be noted downstream of the airport buildings and covers a vertical area about 50 m high, under the nocturnal inversion. The potential temperature superimposed on the wind at 5 m is plotted in Figure 15. An increase of temperature of about 1 K, due to the subsidence area downstream of the buildings, can be clearly observed. This warmer area is propagated downstream and affects an area of more than 500 m in length. This warmer area downstream of the buildings, associated with the increase of TKE, can explain the delay of fog formation in this area. The acceleration/deceleration of the flow and the vertical velocity due to the airport buildings have a strong effect on the turbulence and land–atmosphere exchanges and consequently on the fog formation. They lead to very heterogeneous fog formation over the airport, lasting about 1.5 h.

The characteristics of the fog layer during the mature phase are plotted in Figure 16. The LWP clearly shows that the appearance of KH instabilities is perturbed by the airport buildings. The differences between the airport area and the homogeneous area seem to be due to the impact of buildings on wind shear. The LWC near the ground is also perturbed by the presence of buildings. The subsidence behind the buildings leads to the transport of liquid water towards the ground and consequently to an increase in LWC of about 0.05 g kg^{-1}. However, this has little impact on the horizontal visibility. The vertical cross-section of TKE shows that two areas of TKE production exist: one at ground level close to the buildings and one at the fog top. Even with the presence of buildings, the dynamics of fog still continues to be mainly driven by the process at the fog top. This dynamics at the fog top is mainly decoupled from the ground. The presence of airport buildings has a local impact, but the development and overall characteristics of a fog layer are driven by the processes at its top.

7. Conclusions

Large-eddy simulations of fog over Paris–CdG airport were performed, with the aim of determining the effect of airport buildings on the fog life cycle. In order to study the small-scale three-dimensional structures of the fog layer, simulations were performed at 1 m vertical resolution and 1.5 m horizontal resolution. The largest domain of simulation covered an area of 4.5 km × 1.5 km, which led to a horizontal grid of 3072 × 1014 points. The model was run with an interactive land-surface scheme, with the goal of reproducing the effect of ground heterogeneities on fog.

Three simulations were performed. In the first, the ground was homogeneous and composed only of grass. The second only considered heat transfer through the buildings and runway and friction. Finally, in the third, the blocking effect of the buildings was represented using a drag approach, where buildings were represented by rigid obstacles that were not porous.

With homogeneous ground conditions, the main results of the previous study (Bergot, 2013) were again found. The decreased resolution and increased horizontal domain had little impact on the fog simulation. During the formation phase, a burst of TKE due to KH instabilities suddenly appeared in the surface layer. These KH billows modified the local dynamic conditions and made it easier for the fog to develop in the vertical direction. During the mature phase, the spatial variability of temperature and cloud water content near the ground was small. However, waves were clearly visible at the top of the fog layer, leading to substantial variability of the fog top height. The wind shear across

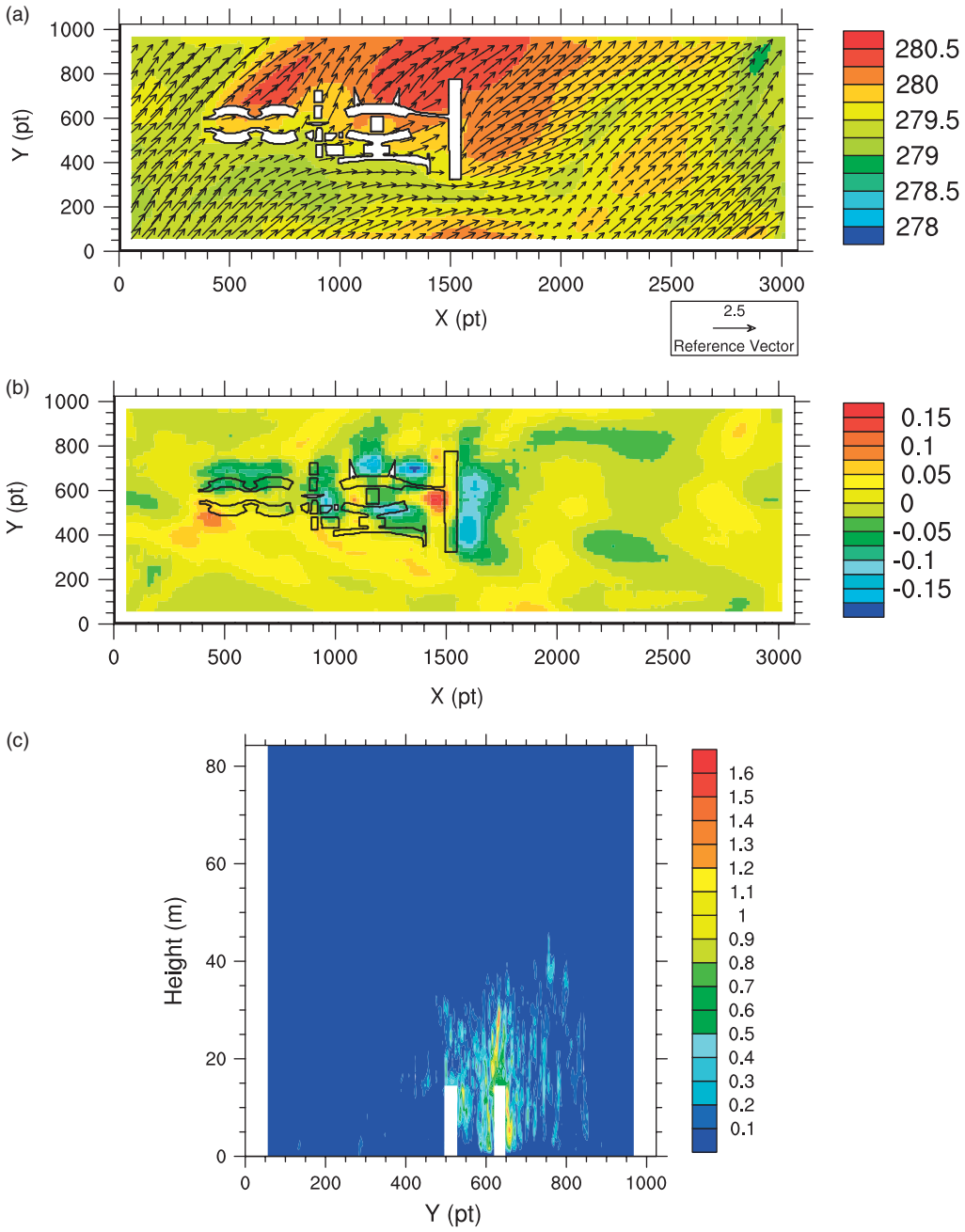

Figure 15. Horizontal cross-section at 2315 UTC for (a) the temperature at 5 m height and (b) the vertical velocity at 30 m height. (c) Vertical cross-section of TKE along the *y*-axis.

the inversion was a major process in the evolution of the fog layer, the dynamics of which were dominated by the processes at its top.

The blocking effect of the airport buildings modified the fog formation strongly. Fog patterns during the formation phase were greatly modified by the presence of the airport area. The fog took 1.5 h to form over the whole simulated airport area. The fog height was also heterogeneous during the formation phase, with the formation of very low clouds. The effect of airport buildings on the vertical velocity could explain the fog height heterogeneities. The airport buildings led to the production of TKE near the ground. This turbulence modification associated with anthropogenic heat release could explain why the fog was heterogeneous during the formation phase.

During the mature phase of the fog, the buildings had little impact on the characteristics of the fog layer. In particular, the increased turbulence helped the development of the fog layer. However, the motions at the top of the fog layer and the wind shear across the inversion were the major processes in the evolution of the fog. This work demonstrates that the fog layer dynamics were mainly controlled by processes at the layer top during the mature phase.

Numerically, this study demonstrates the feasibility and the usefulness of LES in complex terrain for better understanding fog physics. The observations of fog at very fine scale are very poor and this kind of LES simulation can be useful in order better to understand the mechanisms involved in the life cycle of a fog layer. A challenge of great importance is to quantify the relative effect of surface heterogeneities and of fog dynamics on the evolution of a fog layer. In particular, the effect of small-scale structures of a fog layer needs to be observed in future field experiments. Such a LES study can help to plan these field experiements, in order to define the best locations where sensors should be deployed. A challenge of great importance is to observe the formation of KH instabilities in a fog layer.

The goal of this study is not to improve the operational forecast of fog directly. This kind of LES simulation cannot be used from an operational point of view. However, this study shows that the local circulation raises important questions about the forecast of fog formation. These results suggest that the inclusion of high levels of detail in the building representation remains important for the local forecasting of fog formation. Such small-scale ground heterogeneities lead to variability in fog formation and the fog

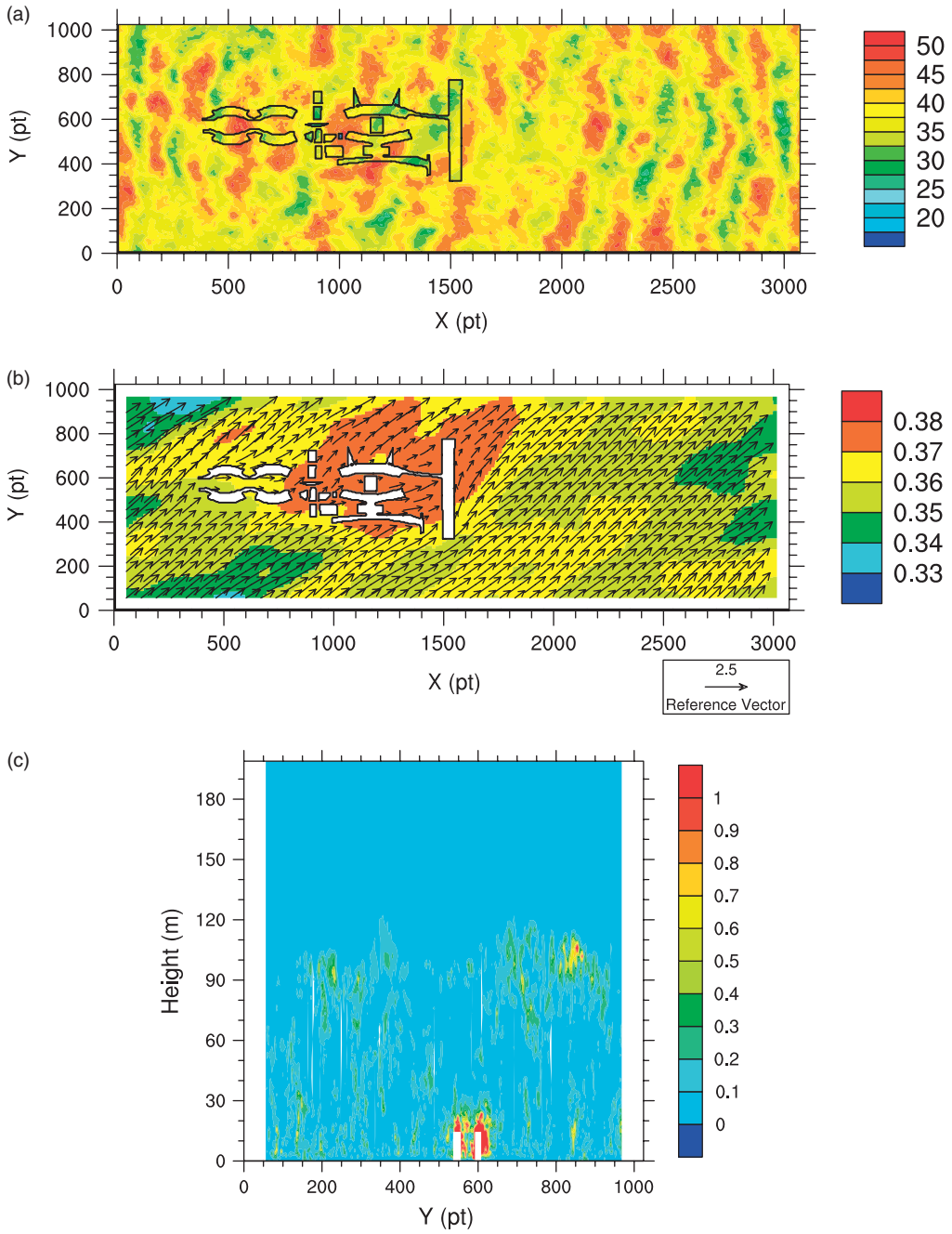

Figure 16. Horizontal cross-section at 0215 UTC for (a) LWP and (b) liquid water content at 5 m. (c) Vertical cross-section of TKE along the *y*-axis.

layer can take about 1 h 30 min to form in the whole airport area. At present, most canopy models included in operational forecasting models do not consider the effect of flow variations due to the buildings. The small-scale variation of the urban canopy has a marked impact on the fog characteristics during its formation. Subgrid spatial variability of the urban canopy seems to be necessary to forecast the local formation of fog accurately, e.g. for an airport. This study also illustrates that a fog forecast over airports needs to include not only the occurrence of fog but also the spatial variability of the fog layer. The spatial variability of fog is also very important during the formation phase and at best can help in planning the reduction of airport capacity.

Acknowledgements

We thank PRACE (project PRACE2011040559) and GENCI (project GENCIt2013017051) for giving us access to resources on the CURIE supercomputer system, located in France at the Très Grand Centre de Calcul (TGCC). The support team of Meso-NH is acknowledged for their help during this study. We acknowledge Aéroport de Paris, who provided us with detailed data of airport buildings. We also thank Lic. Yusvelis Maribel Bàrzaga Ramìrez from the Instituto de Meteorologia, Cuba, for his valuable help with the earlier work on the simulation analysis. We thank the anonymous reviewers for their relevant comments and criticisms.

References

Aumond P, Masson V, Lac C, Gauvreau B, Dupont S, Berengier M. 2013. Including the drag effects of canopies: real case large-eddy simulation studies. *Boundary-Layer Meteorol.* **146**: 65–80.

Beare RJ, MacVean MK. 2004. Resolution sensitivity and scaling of large-eddy simulations of stable boundary layer. *Boundary-Layer Meteorol.* **112**: 257–281.

Bergot T. 2013. Small-scale structure of radiation fog: A large-eddy simulation study. *Q. J. R. Meteorol. Soc.* **139**: 1099–1112.

Bergot T, Guedalia D. 1994. Numerical forecasting of radiation fog. Part I: Numerical model and sensitivity tests. *Mon. Weather Rev.* **122**: 1218–1230.

Bergot T, Carrer D, Noilhan J, Bougeault P. 2005. Improved site-specific numerical prediction of fog and low clouds: A feasibility study. *Weather and Forecasting* **20**: 627–646.

Bergot T, Terradellas E, Cuxart J, Mira A, Liechti O, Mueller M, Nielsen NW. 2007. Intercomparison of single-column numerical models for the prediction of radiation fog. *J. Appl. Meteorol.* **46**: 504–521.

Bott A, Sievers U, Zdunkowski W. 1990. A radiation fog model with a detailed treatment of the interaction between radiative transfer and fog microphysics. *J. Atmos. Sci.* **47**: 2153–2166.

Bou-Zeid E, Overney J, Rogers BD, Parlange MB. 2009. The effects of building representation and clustering in large-eddy simulations of flows in urban canopy. *Boundary-Layer Meteorol.* **132**: 415–436.

Brown MJ. 2000. Urban parametrizations for mesoscale meteorological models. In *Mesoscale Atmospheric Dispersion*, Boybeyi Z. (ed.): 448 pp. WIT press: Wessex Institute of Technologie Press: Southampton, UK.

Carissimo B, Macdonald RW. 2001. 'A porosity/drag approach for the modeling of flox and dispersion in the urban canopy'. In *25th NATO/CCMS International Technical Meeting on Air Pollution Modelling and its Application*, 15–19 October 2001. Louvain la Neuve, Belgique.

Clark DA. 2006. 'Terminal ceiling and visibility product development for northeast airports'. In *Proceedings of the 12th Conference on Aviation, Range and Aerospace Meteorology*. Atlanta, Georgia.

Clark PA, Hopwood WP. 2001. One-dimensional site-specific forcasting of radiation fog. Part I: Model formulation and idealised sensitivity studies. *Meteorol. Appl.* **8**: 279–286.

Cuxart J, Jimenez MA. 2012. Deep radiation fog in a wide closed valley: Study by numerical modeling and remote sensing. *Pure Appl. Geophys.* **169**: 911–926.

Cuxart J, Bougealt P, Redelsperger JL. 2000. A turbulence scheme allowing for mesoscale and large-eddy simulations. *Q. J. R. Meteorol. Soc.* **126**: 1–30.

Deardorff J. 1980. Stratocumulus-capped mixed layers derived from a three dimensional model. *Boundary-Layer Meteorol.* **18**: 495–527.

Duynkerke PG. 1991. Radiation fog: A comparison of model simulation with detailed observations. *Mon. Weather Rev.* **119**: 324–341.

Hamdi R, Masson V. 2008. Inclusion of a drag approach in the Town Energy Balance (TEB) scheme: Offline 1D evaluation in a street canyon. *J. Appl. Meteorol.* **47**: 2627–2644.

Herzegh PH, Bankert RL, Hansen BK, Tryhane M, Wiener G. 2004. 'Recent progress in the development of automated analysis and forecast products for ceiling and visibility conditions'. In *Proceedings of the 20th International Conference on Interactive Information Processing Systems for Meteorology, Oceanography and Hydrology*. Seattle, WA.

Holtslag AAM, Svenson G, Bras P, Basu S, Beare B, Beljars ACM, Bosveld FC, Cuxart J, Ludvall L, Steeneveld GJ, Tjernstrom M, van de Wiel BJH. 2013. Stable boundary layers and diurnal cycles: Challenges for weather and climate models. *Bull. Am. Meteorol. Soc.* **94**: 1691–1706.

Masson V. 2000. A physically-based scheme for the urban energy budget in atmospheric models. *Boundary-Layer Meteorol.* **94**: 357–397.

Masson V, Le Moigne P, Martin E, Faroux S, Alias A, Alkama R, Belamari S, Barbu A, Boone A, Bouyssel F, Brousseau P, Brun E, Calvet J-C, Carrer D, Decharme B, Delire C, Donier S, Essaouini K, Gibelin A-L, Giordani H, Habets F, Jidane M, Kerdraon G, Kourzeneva E, Lafaysse M, Lafont S, Lebeaupin Brossier C, Lemonsu A, Mahfouf J-F, Marguinaud P, Mokhtari M, Morin S, Pigeon G, Salgado R. 2013. The SURFEX v7.2 land and ocean surface platform for coupled or offline simulation of earth surface variables and fluxes. *Geosci. Model Dev.* **6**: 929–960.

Morcrette JJ. 1991. Radiation and cloud radiative properties in the European Centre for Medium Range Weather Forecasts forecasting system. *J. Geophys. Res.* **96**: 9121–9132, doi: 10.1029/89JD01597.

Musson-Genon L. 1987. Numerical simulations of a fog event with a one-dimensional boundary layer model. *Mon. Weather Rev.* **115**: 592–607.

Nakanishi M. 2000. Large-eddy simulation of radiation fog. *Boundary-Layer Meteorol.* **94**: 461–493.

Noilhan J, Planton S. 1989. A simple parametrization of land surface processes for meteorological models. *Mon. Weather Rev.* **117**: 536–549.

Pawlowska H, Brenguier JL. 2000. Microphysical properties of stratocumulus clouds during ACE-2. *Tellus* **52B**: 868–887.

Porson A, Price J, Lock A. 2011. Radiation fog. Part II: Large-Eddy simulation in very stable conditions. *Boundary-Layer Meteorol.* **139**: 193–224.

Rangognio J. 2009. *'Impact des aerosols sur le cycle de vie du brouillard: De l'observation a la modelisation'*, PhD thesis. University Paul Sabatier: Toulouse.

Remy S. 2006. *'Amelioration des parametrisations microphysiques de Meso-NH et Arome pour le brouillard'*. Master's Degree Report M2OASC, note ENM no. 1032. Paul Sabatier University: Toulouse.

Roquelaure S, Tardif R, Remy S, Bergot T. 2009. Skill of a ceiling and visibility local ensemble prediction system (LEPS) according to fog-type prediction at Paris–Charles de Gaulle airport. *Weather and Forecasting* **24**: 1511–1523.

Terradellas E, Bergot T. 2007. Comparison between two single-column models designed for short-term fog and low-clouds forecasting. *Fis. Terra* **19**: 189–203.

Uematsu A, Yamamoto MK, Hashiguchi H, Hirahima K, Fukao S. 2005. Shear-induced roll structure of fog observed by a millimeter-wave scanning Doppler radar. *Geophys. Res. Lett.* **32**: L14824, doi: 10.1029/2005GL022423.

